Biophysical Journal
Article

Biophysical Society

IR Spectroscopy Can Reveal the Mechanism of K^+ Transport in Ion Channels

Steven E. Strong,[1] Nicholas J. Hestand,[1,2] Alexei A. Kananenka,[1,3] Martin T. Zanni,[4] and J. L. Skinner[1,*]
[1]Pritzker School of Molecular Engineering, University of Chicago, Chicago, Illinois; [2]Department of Natural and Applied Sciences, Evangel University, Springfield, Missouri; [3]Department of Physics and Astronomy, University of Delaware, Newark, Delaware; and [4]Department of Chemistry, University of Wisconsin, Madison, Wisconsin

ABSTRACT Ion channels like KcsA enable ions to move across cell membranes at near diffusion-limited rates and with very high selectivity. Various mechanisms have been proposed to explain this phenomenon. Broadly, there is disagreement among the proposed mechanisms about whether ions occupy adjacent sites in the channel during the transport process. Here, using a mixed quantum-classical approach to calculate theoretical infrared spectra, we propose a set of infrared spectroscopy experiments that can discriminate between mechanisms with and without adjacent ions. These experiments differ from previous ones in that they independently probe specific ion binding sites within the selectivity filter. When ions occupy adjacent sites in the selectivity filter, the predicted spectra are significantly redshifted relative to when ions do not occupy adjacent sites. Comparisons between theoretical and experimental peak frequencies will therefore discriminate the mechanisms.

SIGNIFICANCE Ion channels are central to nerve function and are involved in many cellular processes. These channels only permit certain ions to pass through, yet they maintain high passage rates. The mechanism that gives rise to this behavior is hotly debated. Here, we use theoretical predictions of infrared spectroscopy to propose an experiment that will discriminate between two proposed mechanisms. This paper also serves as a proof of principle for a general approach to studying protein function in an aqueous environment, in which theoretical spectroscopy is used to design infrared experiments.

INTRODUCTION

Ion channels are essential to cell function (1). They facilitate the selective and rapid transport of ions across the cell membrane and, in combination with ATP-driven pumps, regulate the membrane potential. The membrane potential is an important cellular energy storage mechanism and is also used to transmit signals, e.g., in neurons. While sodium and potassium, both monovalent cations, have the same effect on the membrane potential, cells often make use of these ions in different ways, requiring ion channels to distinguish them. For example, the membrane potential spike that transmits signals in neurons is driven at first by sodium influx, whereas the subsequent fast repolarization is driven by potassium efflux (1). Sodium and potassium ions, with the same charge and similar ionic radii (0.95 and 1.33 Å), would appear to be difficult to distinguish, yet ion channels facilitate selective transport at near diffusion-limited rates (2). Despite decades of research (2–18), it remains unclear what ion conduction mechanism underpins this feat.

The potassium ion channel KcsA (K^+ channel of streptomyces A) serves as a model system for ion channel studies (19,20). KcsA is composed of four identical subunits surrounding a central pore (Fig. 1 *a*) (21,22). The part of the protein thought to be responsible for K^+ selectivity is called the "selectivity filter" and is on the extracellular side of the protein (21). Ions in the selectivity filter are coordinated by the protein's backbone carbonyl oxygens (11,23,24), which are arranged to form five binding sites denoted S0–S4 (Fig. 1 *b*) (2,22,25). The protein rectifies ion current out of the cell (26,27), so most ion passage events begin when an ion enters the channel at S4 and end when an ion leaves the channel on the extracellular side at S0. The details of the mechanism between these steps, and how they simultaneously enable selectivity and fast transport, are still debated.

Submitted September 17, 2019, and accepted for publication November 12, 2019.

*Correspondence: jlskinner@uchicago.edu
Steven E. Strong and Nicholas J. Hestand contributed equally to this work.

Editor: Vasanthi Jayaraman.
https://doi.org/10.1016/j.bpj.2019.11.013

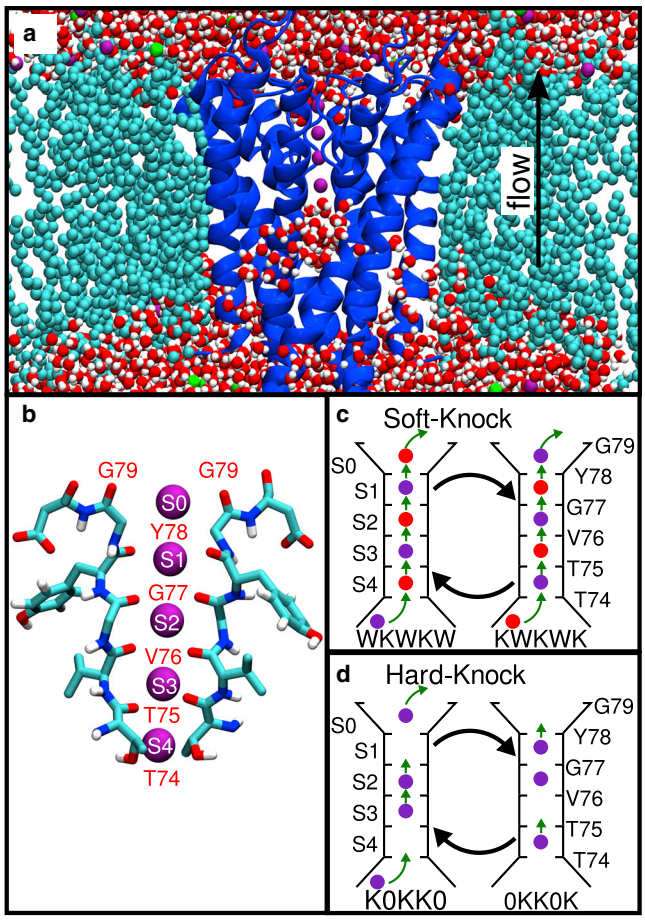

FIGURE 1 (*a*) An image from one of the molecular dynamics trajectories shows the KcsA protein (*blue*) spanning the lipid membrane (*cyan*). The membrane is immersed in water (*red/white*) with dissolved potassium (*purple*) and chloride (*green*) ions. The selectivity filter with ions in sites S1–S4 can be seen in the middle. During ion conduction, potassium ions flow from the cell (*bottom*) to the extracellular medium (*top*). (*b*) A close-up of two of the four protein segments that comprise the selectivity filter shows the five ion sites (S0–S4) and the six carbonyl oxygens (*red*). (*c*) A schematic of the soft-knock mechanism showing the alternating occupation of potassium ions (*purple*) and water molecules (*red*) is shown. Ion conduction proceeds when the whole chain translocates by one site (*green arrows*). In the hard-knock mechanism, ion passage occurs according to the green arrows in (*d*). See the text for more detail. To see this figure in color, go online.

Several possible mechanisms have been put forward (4,14,25,28–34), most of which are "knock-on" mechanisms. In this class of mechanisms, an incoming ion knocks against the entrance to the selectivity filter, advancing its contents and expelling an ion from the other side. The leading variant of these mechanisms, supported by crystallographic evidence (21,31), asserts that this knock-on effect is mediated by water molecules because direct ion-ion contacts might be energetically unfavorable (25,29–31). Here, we call this the "soft-knock" mechanism to distinguish it from the alternative "hard-knock" mechanism described by Köpfer et al., in which the knock-on effect occurs directly between ions (14).

According to the soft-knock mechanism, the sites S0–S4 are always occupied by an alternating sequence of ions and water molecules. The selectivity filter fluctuates between the two occupation states shown in Fig. 1 *c* until an ion enters the channel from the cell, shifting this equilibrium so that an ion is pushed out the other side. In addition to the crystallographic evidence mentioned above (21,31), the soft-knock mechanism is also supported by streaming-potential measurements that suggest that water is transported along with ions in the channel (29,33,35), as well as theoretical work (25,28,30). The hard-knock mechanism, on the other hand, starts with ions in S2 and S3 (Fig. 1 *d*) (14). When a new ion enters the channel at S4, ion-ion repulsion knocks the pair of ions at S2-S3 up to S1-S2. The ion in S1 exits the channel by moving into S0, and the ion in S4 moves up to S3, restoring the initial state with ions at S2-S3. This mechanism is supported by a nonequilibrium molecular dynamics (MD) simulation that observed the mechanism with atomistic detail, a reinterpretation of the crystallographic evidence (14), and solid-state NMR experiments (36). The hard-knock mechanism also explains the selectivity of the channel through the increased energetic cost of completely desolvating a sodium ion compared with a potassium ion (17). In the soft-knock mechanism, this effect is less pronounced because ions in the selectivity filter are only partially desolvated, although the smaller effect may still explain the observed selectivity.

Several techniques have been used to try to resolve this controversy. Crystallography seems like the natural choice because of its spatial resolution, but it is unable to distinguish the mechanisms because the measurement captures an ensemble average of the ion occupation states. Recent advances in time-resolved crystallography promise to resolve ion positions during the transport process (37), but this approach can only probe crystalline samples. Other researchers have used solid-state NMR, which permits noncrystalline samples but still requires solid aggregates and is not applicable to aqueous solutions (36). Solution NMR relaxes this constraint but uses nonnative ions because of the broad linewidth of K^+ signals (13). Infrared (IR) spectroscopy, on the other hand, can probe the selectivity filter in a natural, cell-membrane-like environment with the native K^+ ion (38). In this approach, one commonly focuses on the amide I stretching mode, which is dominated by the stretching motion of the carbonyl group (39–44). Replacing carbonyl groups with $^{13}C^{18}O$ isotope labels redshifts the amide I frequency by 65 cm^{-1}, spectroscopically isolating it from the other amide I stretches in the protein and enabling selective probing of specific binding sites in the selectivity filter (45,46). A similar methodology has been applied to study the impact of gating on the selectivity filter (47). Like crystallography, IR spectroscopy also captures an ensemble average of ion occupation states, but crucially, the ability to accurately compute IR spectra from MD simulations allows one to decompose the ensemble average into its component pieces.

In 2016, Kratochvil et al. leveraged this approach to experimentally probe the mechanism of ion transport in KcsA using two-dimensional (2D) IR spectroscopy and isotope labels on three amino acids (V76, G77, and G79) in the selectivity filter (16). They then fit the experimental spectrum of the labeled KcsA protein using calculated spectra of the occupation states relevant to either the hard-knock or soft-knock mechanisms shown in Fig. 1, *c* and *d*. They were able to fit the spectrum with the soft-knock occupation states but not the hard-knock states, so they concluded that the soft-knock mechanism is consistent with the experiment, whereas the hard-knock mechanism is not (16). Later, Kopec et al. found that a larger set of hard-knock occupation states, including those with a water molecule in S1, do fit the 2D IR data (17). Because of the large number of possible occupation states consistent with each mechanism, especially the hard-knock mechanism, the fit to existing 2D IR data is not constrained enough to test for adjacent ions, which is a key discrepancy between the two mechanisms. This does not, however, rule out the possibility that IR spectroscopy might distinguish the mechanisms experimentally. Kratochvil et al. only studied one possible choice of isotope labels (V76-G77-G79). Many other possible combinations exist that may shed more light on the transport mechanism. The experiments are tractable but time-consuming, so it is useful for computation to guide experiments by predicting which isotope labels best discriminate the two mechanisms.

Here, we compute IR spectra for single isotope labels at all sites inside the filter (T75, V76, G77, Y78, and G79) as well as for some combinations of double and triple labels (data not shown). Based on this data set, we propose a set of experiments that can distinguish the two mechanisms. Specifically, we find that single labels at V76 and G77 are able to distinguish the two mechanisms. This is likely because these labels probe sites near the middle of the filter, where the hard-knock mechanism and soft-knock mechanism differ most starkly. The hard-knock mechanism predicts that there are two adjacent ions in this region, whereas the soft-knock mechanism predicts that there are never adjacent ions. The electrostatic attraction between the K^+ ions and the electronegative carbonyl oxygen weakens the carbonyl bond, resulting in lower vibrational frequencies. When a carbonyl oxygen coordinates two ions at once, its frequency redshifts more dramatically than when it coordinates only one ion or an ion and a water molecule. In the hard-knock mechanism, both the V76 and G77 carbonyls can coordinate two ions at once (Fig. 1 *d*). In the soft-knock mechanism, on the other hand, this never happens (Fig. 1 *c*). One expects that labels at the V76 and G77 amide units will be sensitive to this difference between the mechanisms and, therefore, capable of discriminating them. The T75, Y78, and G79 carbonyls, on the other hand, are never doubly coordinated by ions in the hard-knock mechanism, so there is less of a difference in their spectra between the two mechanisms.

Using singly-labeled proteins with labels at the V76 and G77 carbonyls, we compute the spectrum for each possible occupation state of the selectivity filter. The experimental IR spectrum, however, is a weighted average of all the occupation states that are visited at equilibrium. Because the mechanism is unknown, these weights are also unknown. MD or Monte Carlo simulations cannot elucidate the weights for several reasons: First, transport is rare at equilibrium, so sampling is difficult, and the results may depend strongly on initial conditions (18,48). Nonequilibrium and enhanced sampling techniques have been applied to overcome this problem, but the results depend on which technique is used (14,25,30). Furthermore, it is unclear how the nonequilibrium weights relate to the equilibrium ones (16,17,49). Finally, many force fields exist for biophysical simulations, but none are known to generate the correct weights for this problem, and the results are probably sensitive to the choice of force field (18,50). Therefore, a proposed experiment that discriminates between the hard-knock and soft-knock mechanisms must be able to do so for any possible set of weights.

Although the schematic descriptions of each mechanism involve only two occupation states each (Fig. 1, *c* and *d*), there are likely many other states that are visited as transition states, longer-lived intermediates, or fluctuations that are unproductive from a transport standpoint. Such auxiliary states are likely more prevalent in the hard-knock mechanism because of the vacancies in the selectivity filter that allow more room for movement. This wide array of states results in a correspondingly large space of possible weights. The majority of the variability in possible states occurs near the edges of the channel, especially sites S0, S1, and S4 (17). We reduce the experimental sensitivity to this variability by focusing on labels in the center of the channel. We can then consider only the two characteristic states shown in Fig. 1, *c* and *d*, eliminating the complexity arising from the large space of possible states. In this much smaller space, it is tractable to propose experiments that discriminate the two mechanisms for any possible set of weights.

METHODS

We calculate the linear and ZZZZ polarized 2D IR spectra using the NISE3 program (51–55) following the prescription used in (16), with minor modifications. In (16), the linear and third-order response functions were calculated to maximum coherence times of 5 ps. We calculate the linear and third-order response functions to maximum coherence times of 10 ps to avoid any artifacts due to ringing. The Hamiltonian and dipole trajectories are calculated from classical MD simulations of the KcsA channel using the spectroscopic maps in (56,57) with the parameters discussed in (16). Note that the charges on the ions were scaled according to ab initio calculations (58), as discussed in (16). The MD trajectories are the same as those used by Kratochvil et al. to calculate the spectra (16). For some of these trajectories, restraints on the ion positions were used to prevent interconversion between occupation states. See (16) for details. We compute the theoretical spectra for the four representative occupation states in Fig. 1, *c* and *d* using single labels at both V76 and G77. We also calculate the spectra for the system

with a triple label at V76, G77, and G79 to ensure consistency with previous studies (data not shown).

The occupation states are labeled by a string of five characters that indicates the occupation of each of the five sites S0–S4. A "K" indicates occupation by a potassium ion, a "W" indicates occupation by a water molecule, and a "0" indicates a vacancy. For example, the label K0KK0 indicates that there is a potassium ion in sites S0, S2, and S3 and vacancies at the other sites. The four occupation states we study are K0KK0, 0KK0K, WKWKW, and KWKWK. Note that water sometimes occupies the S4 site in the K0KK0 state, transiently converting it to K0KKW. We ignore this effect here, treating transient K0KKW states as K0KK0 states.

RESULTS AND DISCUSSION

We predict that two experiments, one with a V76 label and one with a G77 label, will discriminate between the soft-knock and hard-knock mechanisms. For a given label, we calculate the spectra for each mechanism using weighted combinations of the spectra for the two representative occupation states of the selectivity filter (Fig. 1, *c* and *d*). Because the true weighting is unknown, we tune the weighting parameter between the two states to ensure that the proposed experiments distinguish between the two mechanisms for any choice of weight (Figs. 2 and 3).

The spectra of the hard-knock mechanism are distinguished by a redshift relative to the soft-knock mechanism. As mentioned above, the electric field of the ions weakens the carbonyl bond, thereby lowering the vibrational frequency of the amide I stretch. Because there are more ions near the labeled carbonyls for the hard-knock mechanism, the electric field is enhanced, and the vibrational frequencies are lower. Water molecules also redshift the amide I stretching frequencies due to hydrogen bonding (45,56,59–62), but to a lesser degree than the ions do.

The accuracy of the spectroscopic maps have been tested in the case of a gas-phase polypeptide, in which the average unsigned error was less than 4 cm^{-1}, and the largest error was only 11 cm^{-1} (63). Here, the environment is not gas phase, but the spectral shifts in question are, for the most part, considerably larger than these errors (63). For some choices of weights, the shift between the hard- and soft-knock spectra approaches our confidence in the maps. For example, the G77-labeled pure K0KK0 hard-knock

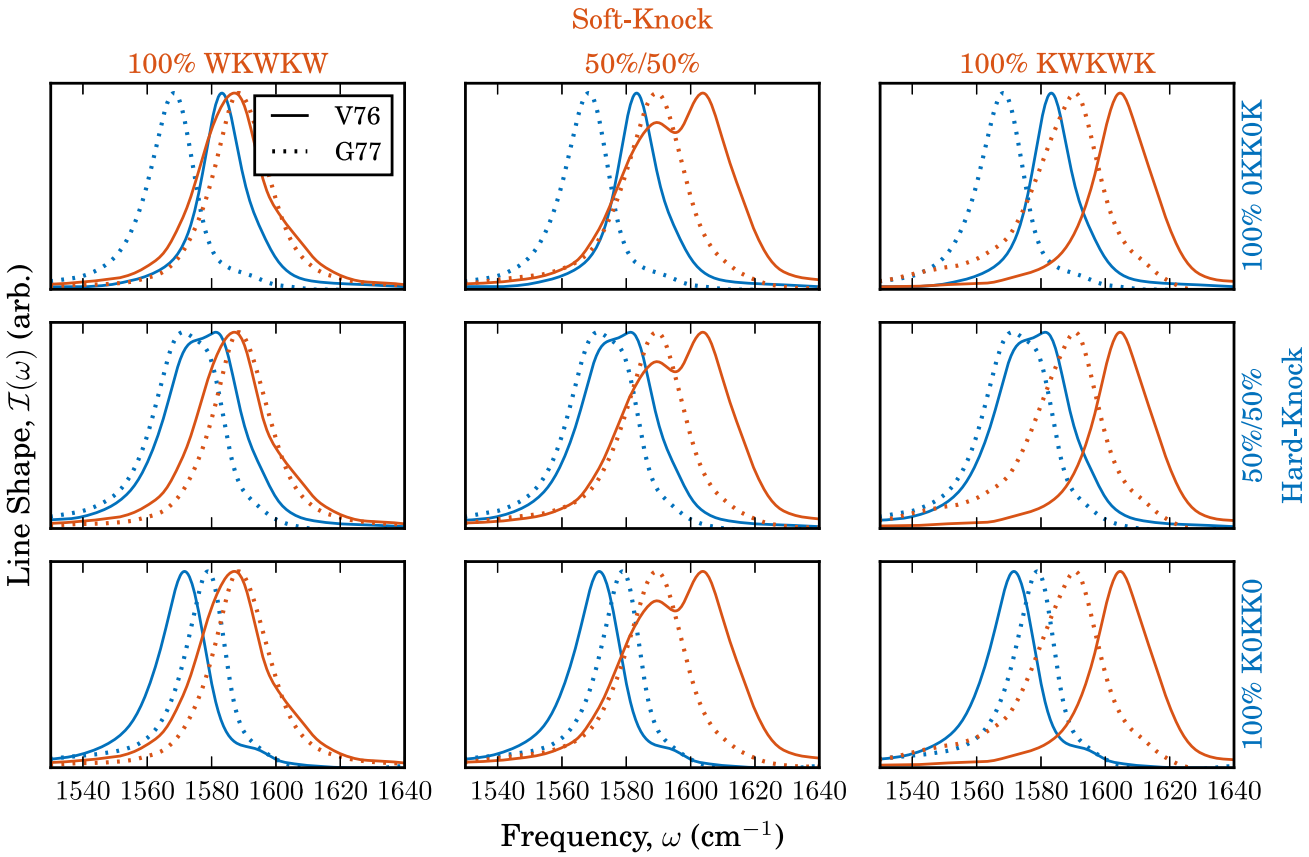

FIGURE 2 A comparison of the linear IR spectra of the two mechanisms for nine possible combinations of weights. The occupation states WKWKW, KWKWK, K0KK0, and 0KK0K are defined in Fig. 1, *c* and *d*. The redshift of the hard-knock spectra relative to the soft-knock ones always distinguishes the two mechanisms. For some labels and weights, like the V76-labeled spectrum in the upper-left corner or the G77-labeled spectrum in the lower right, the redshift is as small as ~5–10 cm^{-1}, which does not distinguish the mechanisms within the error of the map. But in these cases, the other label always distinguishes the two mechanisms very easily. In some cases, the mechanisms can also be distinguished by the qualitative appearance of a double peak as well as the redshift. To see this figure in color, go online.

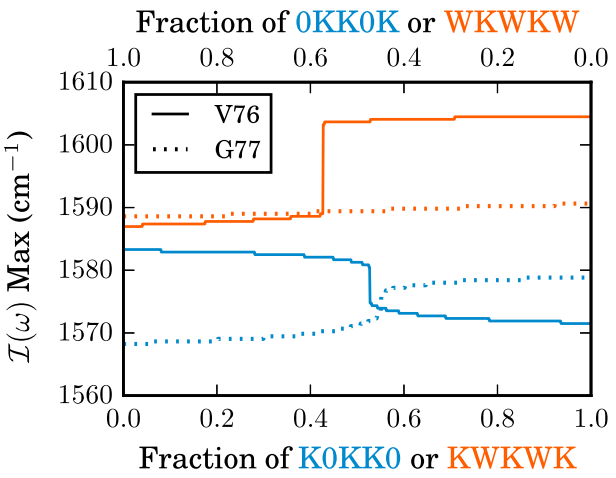

FIGURE 3 The peak frequency as a function of weight between the two representative occupation states for the hard-knock (*blue*) and soft-knock (*orange*) mechanisms. For any given weight, at least one of the single labels predicts a frequency difference larger than our uncertainty in the spectroscopic maps. To see this figure in color, go online.

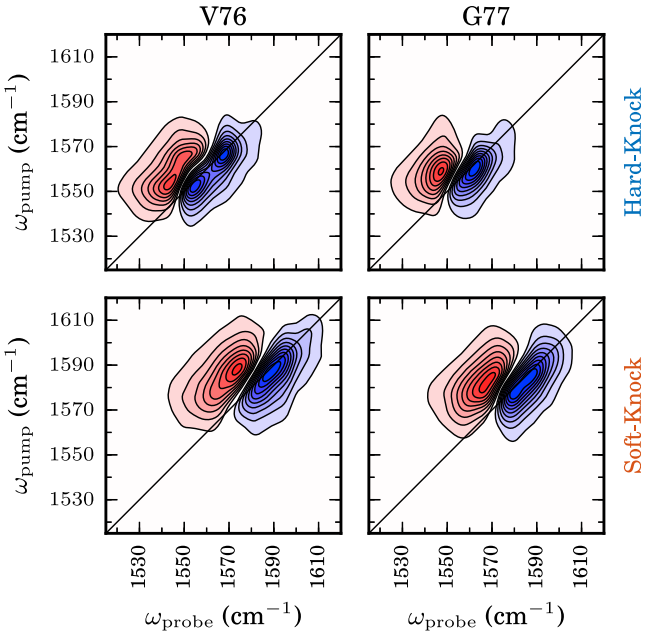

FIGURE 4 The 2D IR spectra for the 50/50% mixture of the hard-knock spectra (*top*) are distinguishable from the 50/50% mixture of the soft-knock spectra (*bottom*). The hard-knock spectra are redshifted by over 20 cm^{-1} relative to the soft-knock ones and show a double peak along the diagonal as well in the case of the V76 label. These four spectra are the 2D equivalents of those in the central panel in Fig. 2. As for the linear IR spectra, the 2D IR spectra can distinguish the mechanism for all possible combinations of weights, although only one choice of weight is shown here for brevity. To see this figure in color, go online.

spectrum is only ∼10 cm^{-1} redshifted from the pure KWKWK soft-knock spectrum (lower right, Fig. 2). Likewise, the V76-labeled pure 0KK0K hard-knock spectrum is only ∼5 cm^{-1} redshifted from the pure WKWKW soft-knock spectrum (upper left, Fig. 2). In both of these cases, however, the other label gives a redshift of ∼20–35 cm^{-1}, easily distinguishing the mechanisms. Thus, although each single label independently is not enough to distinguish the mechanisms regardless of the weights, combined they are sufficient (Fig. 3). In some weighting regimes, the V76-labeled spectrum of the hard-knock mechanism presents a double peak, whereas the soft-knock mechanism does not, providing another distinguishing feature.

Fig. 2 presents the linear IR spectra for ease of comparison, but in practice, 2D IR spectroscopy has advantages in terms of structural sensitivity as well as frequency and time resolution (64,65). Fig. 4 shows the 2D IR spectra for the equal-weight case (50%/50%) for both mechanisms. They are distinguishable by the same features as discussed for the linear IR spectra: a redshift for both labels and a double peak along the diagonal for the V76 label. These conclusions hold for all the 2D IR spectra for any combination of weights. We only show one possibility here for brevity.

We have also verified that the triple label used in the Kratochvil et al. experiment does not distinguish the two mechanisms using the same logic, in agreement with Kopec et al. (data not shown) (17). The triple label fails to distinguish the mechanisms for two reasons. First, the approach to distinguishing the mechanisms described above requires addressing the two different labels independently. The triple label combines this information in a way that cannot be disentangled. Second, the triple label includes a G79 label. This label probes the S0 site, but the S0 site is at the extracellular edge of the selectivity filter, and the G79 carbonyl points into the aqueous extracellular environment. So any information about the occupation of the S0 site is convoluted with unhelpful information about the water outside the cell, as mentioned in the supplemental text of (16). Furthermore, the S0 site is larger and more poorly defined than the other sites (25), and it is at the edge of the selectivity filter, so its dynamics may be on a different timescale than those inside the channel. The occupation of S0 appears to be well-defined by the two proposed mechanisms in Fig. 1, *c* and *d*, but in reality, neither mechanism describes its dynamics in any detail.

Indeed, Kopec et al. find several other occupancy states in equilibrium MD simulations that only differ from the K0KK0 state by the occupations of the S0 and S1 sites (17). If the ion in S0 diffuses away from the selectivity filter on a faster timescale than the transport process shown in Fig. 1 *d*, then water molecules can occupy the S0 and S1 sites transiently, making the states WWKK0, 0WKK0, W0KK0, and 00KK0. The KWKK0 state could also be observed when the ion in S0 allows a water molecule into the channel before diffusing away. Likewise, in the soft-knock mechanism, the KWKWK state could transiently convert to 0WKWK, WWKWK, W0WKW, or 00KWK. By forgoing a label at G79, we attempt to lessen the impact

of the occupancy of S0 on the final spectra because it is poorly understood in both proposed mechanisms. As just shown, however, the occupancy of S1 is also somewhat uncertain and may transiently fluctuate between 0 and W. To check that our conclusions are robust to this uncertainty, we repeat the same analysis shown in Fig. 2, replacing the K0KK0 state with KWKK0 (data not shown). The same logic used above still discriminates between the mechanisms.

In addition to the wide array of possible occupation states, the protein may also adopt different configurations. For example, MD simulations of KcsA have observed a configuration in which one carbonyl group flips away from the interior of the selectivity filter (66–70). This configuration is nonconductive (17,71), but it may still be relevant at the equilibrium conditions in which the experiments are conducted. Existing crystallographic data do not support the existence of the flipped configuration (21,22,31), so it has been ignored in the above analysis, but previous efforts to determine the transport mechanism have relied on its existence. Kratochvil et al. found that the soft-knock mechanism was compatible with their experimental 2D IR spectrum, but only if this flipped configuration is included in the analysis (16). Therefore, an experimental test of the existence of this flipped configuration may provide another way to distinguish the two mechanisms.

Kratochvil et al. found that, to fit their experimental spectrum, they needed to include the flipped configuration for the WKWKW state with weights of ∼3:3:4 KWKWK:WKWKW:WKWKW(flipped). We compare the weighted linear IR spectrum both with and without the flipped configuration, and find a signature of the flipped configuration by extending the spectral window to higher frequencies than previously considered. The spectrum with the flipped configuration included has a pronounced peak at ∼1640 cm^{-1}, where there is no corresponding feature in the spectrum without the flipped configuration (Fig. 5). Experimental observation of this feature would not support either the hard-knock or soft-knock mechanism but would be an interesting development for the hypothesis that the flipped configuration plays a role in gating the channel (66). If experiments are unable to observe this feature, on the other hand, this may suggest that the flipped configuration is an artifact of the force fields used in MD simulations. Without the flipped configuration, the soft-knock mechanism cannot explain the experimental 2D IR spectrum by Kratochvil et al. (16), because the flipped configuration was instrumental in achieving agreement between the theoretical soft-knock spectrum and the experimental spectrum. This 1640 cm^{-1} feature may be difficult to observe experimentally, however, because of its overlap with the band of unlabeled amide I vibrations. It may be possible to observe when the residue is not isotope labeled, which would put its frequency at ∼1706 cm^{-1}, and so would lie on the high-frequency side of the amide I band.

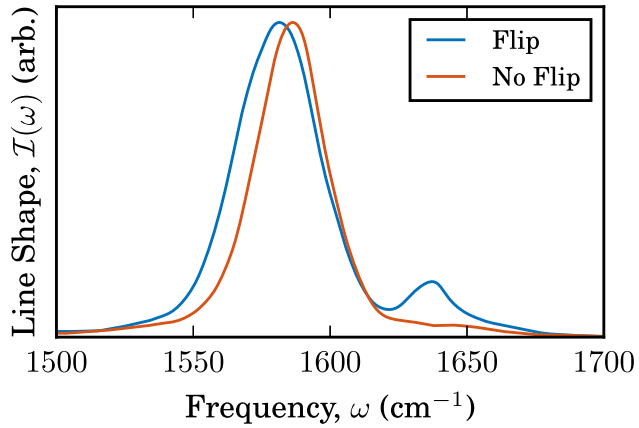

FIGURE 5 Trajectories with a flipped V76 label show a spectroscopic feature at ∼1640 cm^{-1}. This feature could permit an experimental test of the existence of this configuration. These spectra are composed according to the weights in Kratochvil et al. (16) because that study relies on the existence of the flipped configuration to support the soft-knock mechanism. The spectrum with the flipped configuration (*blue*) is composed of 3:3:4 KWKWK/WKWKW/WKWKW(flipped), whereas the spectrum without the flipped configuration (*orange*) is 1:1 KWKWK/WKWKW. To see this figure in color, go online.

CONCLUSIONS

Understanding the ion occupation states that exist within the selectivity filter is central to understanding selective K^+ transport. Here, we propose two experiments that, in combination, can distinguish between the soft-knock and hard-knock mechanisms by testing for adjacent ions. The experiments we propose are challenging and time consuming, but they are not more technically difficult than those performed by Kratochvil et al. (16), and they are currently in progress in the Zanni group. In both suggested experiments, adjacent ions in the hard-knock occupation states redshift the IR spectra relative to the soft-knock spectra. For some occupancy weights, the redshifts obtained from each label independently are not large enough to distinguish the mechanisms. When both labels are considered simultaneously, however, at least one label gives a large enough redshift to distinguish the mechanisms for any choice of weight. Hence, one can discriminate the mechanisms by simply comparing the experimental peak frequencies to the theoretical predictions (Fig. 3). Finally, we find a spectroscopic signature of the flipped configuration. Experimental observation of this feature would not help distinguish the mechanisms, but its absence would suggest that the soft-knock mechanism is not correct.

Although our work focuses on KcsA, the same question about the ion transport mechanism is now arising in other ion channels, including NaK and NaK2K (17,72). The approach we describe here can be applied to those systems as well, promising to resolve the significant and fascinating problem of ion transport across the cell membrane. More broadly, this approach can be applied to large classes of

biophysical problems in which conflicting mechanisms have been proposed. Critical to this advance is the ability to accurately calculate IR spectra from MD simulations. This capability, enabled by the short duration (∼ps) of vibrational lifetimes, is unique to IR spectroscopy and provides an important link between experiments and the atomistic detail available in MD simulations.

AUTHOR CONTRIBUTIONS

All authors designed the research. S.E.S. and N.J.H. computed the spectra and wrote the manuscript.

ACKNOWLEDGMENTS

We thank Joshua Carr and Michał Maj for providing MD trajectories of the KcsA channel.

This work was completed in part with resources provided by the University of Chicago Research Computing Center, the Pritzker School of Molecular Engineering, and the National Institutes of Health, National Institute of Diabetes and Digestive and Kidney Disease (NIDDK) ROI DK087985. Zanni is co-owner of PhaseTech Spectroscopy, which sells 2D IR spectrometers.

REFERENCES

1. Hille, B. 2001. Ion Channels of Excitable Membranes, Third Edition. Sinauer Associates, Inc, Sunderland, MA.
2. MacKinnon, R. 2004. Potassium channels and the atomic basis of selective ion conduction (Nobel Lecture). *Angew. Chem. Int. Ed. Engl.* 43:4265–4277.
3. Hodgkin, A. L., and A. F. Huxley. 1952. A quantitative description of membrane current and its application to conduction and excitation in nerve. *J. Physiol.* 117:500–544.
4. Hodgkin, A. L., and R. D. Keynes. 1955. The potassium permeability of a giant nerve fibre. *J. Physiol.* 128:61–88.
5. Hille, B. 1970. Ionic channels in nerve membranes. *Prog. Biophys. Mol. Biol.* 21:1–32.
6. Armstrong, C. M. 1971. Interaction of tetraethylammonium ion derivatives with the potassium channels of giant axons. *J. Gen. Physiol.* 58:413–437.
7. Neher, E., and B. Sakmann. 1976. Single-channel currents recorded from membrane of denervated frog muscle fibres. *Nature.* 260:799–802.
8. Armstrong, C. M. 1981. Sodium channels and gating currents. *Physiol. Rev.* 61:644–683.
9. Tempel, B. L., D. M. Papazian, …, L. Y. Jan. 1987. Sequence of a probable potassium channel component encoded at Shaker locus of Drosophila. *Science.* 237:770–775.
10. Heginbotham, L., T. Abramson, and R. MacKinnon. 1992. A functional connection between the pores of distantly related ion channels as revealed by mutant K^+ channels. *Science.* 258:1152–1155.
11. Heginbotham, L., Z. Lu, …, R. MacKinnon. 1994. Mutations in the K^+ channel signature sequence. *Biophys. J.* 66:1061–1067.
12. Thompson, A. N., I. Kim, …, C. M. Nimigean. 2009. Mechanism of potassium-channel selectivity revealed by Na^+ and Li^+ binding sites within the KcsA pore. *Nat. Struct. Mol. Biol.* 16:1317–1324.
13. Eichmann, C., L. Frey, …, R. Riek. 2019. Probing ion binding in the selectivity filter of the KcsA potassium channel. *J. Am. Chem. Soc.* 141:7391–7398.
14. Köpfer, D. A., C. Song, …, B. L. de Groot. 2014. Ion permeation in K^+ channels occurs by direct Coulomb knock-on. *Science.* 346:352–355.
15. Ahern, C. A., J. Payandeh, …, B. Chanda. 2016. The hitchhiker's guide to the voltage-gated sodium channel galaxy. *J. Gen. Physiol.* 147:1–24.
16. Kratochvil, H. T., J. K. Carr, …, M. T. Zanni. 2016. Instantaneous ion configurations in the K^+ ion channel selectivity filter revealed by 2D IR spectroscopy. *Science.* 353:1040–1044.
17. Kopec, W., D. A. Köpfer, …, U. Zachariae. 2018. Direct knock-on of desolvated ions governs strict ion selectivity in K^+ channels. *Nat. Chem.* 10:813–820.
18. Flood, E., C. Boiteux, …, T. W. Allen. 2019. Atomistic simulations of membrane ion channel conduction, gating, and modulation. *Chem. Rev.* 119:7737–7832.
19. Schrempf, H., O. Schmidt, …, R. Wagner. 1995. A prokaryotic potassium ion channel with two predicted transmembrane segments from Streptomyces lividans. *EMBO J.* 14:5170–5178.
20. Schrempf, H. 2005. Deciphering Streptomyces lividans KcsA as a K channel model. *In* Bacterial Ion Channels and Their Eukaryotic Homologs. A. Kubalski and B. Martinac, eds. ASM Press, pp. 41–68.
21. Doyle, D. A., J. Morais Cabral, …, R. MacKinnon. 1998. The structure of the potassium channel: molecular basis of K^+ conduction and selectivity. *Science.* 280:69–77.
22. Zhou, Y., J. H. Morais-Cabral, …, R. MacKinnon. 2001. Chemistry of ion coordination and hydration revealed by a K^+ channel-Fab complex at 2.0 Å resolution. *Nature.* 414:43–48.
23. Bezanilla, F., and C. M. Armstrong. 1972. Negative conductance caused by entry of sodium and cesium ions into the potassium channels of squid axons. *J. Gen. Physiol.* 60:588–608.
24. Hille, B. 1973. Potassium channels in myelinated nerve. Selective permeability to small cations. *J. Gen. Physiol.* 61:669–686.
25. Bernèche, S., and B. Roux. 2001. Energetics of ion conduction through the K^+ channel. *Nature.* 414:73–77.
26. Meuser, D., H. Splitt, …, H. Schrempf. 1999. Exploring the open pore of the potassium channel from *Streptomyces lividans*. *FEBS Lett.* 462:447–452.
27. LeMasurier, M., L. Heginbotham, and C. Miller. 2001. KcsA: it's a potassium channel. *J. Gen. Physiol.* 118:303–314.
28. Åqvist, J., and V. Luzhkov. 2000. Ion permeation mechanism of the potassium channel. *Nature.* 404:881–884.
29. Morais-Cabral, J. H., Y. Zhou, and R. MacKinnon. 2001. Energetic optimization of ion conduction rate by the K^+ selectivity filter. *Nature.* 414:37–42.
30. Bernèche, S., and B. Roux. 2003. A microscopic view of ion conduction through the K^+ channel. *Proc. Natl. Acad. Sci. USA.* 100:8644–8648.
31. Zhou, Y., and R. MacKinnon. 2003. The occupancy of ions in the K^+ selectivity filter: charge balance and coupling of ion binding to a protein conformational change underlie high conduction rates. *J. Mol. Biol.* 333:965–975.
32. Furini, S., and C. Domene. 2009. Atypical mechanism of conduction in potassium channels. *Proc. Natl. Acad. Sci. USA.* 106:16074–16077.
33. Iwamoto, M., and S. Oiki. 2011. Counting ion and water molecules in a streaming file through the open-filter structure of the K channel. *J. Neurosci.* 31:12180–12188.
34. Fowler, P. W., E. Abad, …, M. S. Sansom. 2013. Energetics of multi-ion conduction pathways in potassium ion channels. *J. Chem. Theory Comput.* 9:5176–5189.
35. Alcayaga, C., X. Cecchi, …, R. Latorre. 1989. Streaming potential measurements in $Ca2^+$-activated K^+ channels from skeletal and smooth muscle. Coupling of ion and water fluxes. *Biophys. J.* 55:367–371.
36. Öster, C., K. Hendriks, …, A. Lange. 2019. The conduction pathway of potassium channels is water free under physiological conditions. *Sci. Adv.* 5:eaaw6756.

37. Hekstra, D. R., K. I. White, …, R. Ranganathan. 2016. Electric-field-stimulated protein mechanics. *Nature.* 540:400–405.

38. Ataka, K., T. Kottke, and J. Heberle. 2010. Thinner, smaller, faster: IR techniques to probe the functionality of biological and biomimetic systems. *Angew. Chem. Int. Ed. Engl.* 49:5416–5424.

39. Krimm, S., and J. Bandekar. 1986. Vibrational spectroscopy and conformation of peptides, polypeptides, and proteins. *Adv. Protein Chem.* 38:181–364.

40. Jackson, M., and H. H. Mantsch. 1995. The use and misuse of FTIR spectroscopy in the determination of protein structure. *Crit. Rev. Biochem. Mol. Biol.* 30:95–120.

41. Hamm, P., M. Lim, and R. M. Hochstrasser. 1998. Structure of the amide I band of peptides measured by femtosecond nonlinear-infrared spectroscopy. *J. Phys. Chem. B.* 102:6123–6138.

42. Barth, A., and C. Zscherp. 2002. What vibrations tell us about proteins. *Q. Rev. Biophys.* 35:369–430.

43. DeCamp, M. F., L. DeFlores, …, M. Cho. 2005. Amide I vibrational dynamics of N-methylacetamide in polar solvents: the role of electrostatic interactions. *J. Phys. Chem. B.* 109:11016–11026.

44. Feng, C. J., and A. Tokmakoff. 2017. The dynamics of peptide-water interactions in dialanine: an ultrafast amide I 2D IR and computational spectroscopy study. *J. Chem. Phys.* 147:085101.

45. Wang, L., C. T. Middleton, …, J. L. Skinner. 2011. Development and validation of transferable amide I vibrational frequency maps for peptides. *J. Phys. Chem. B.* 115:3713–3724.

46. Leisle, L., F. Valiyaveetil, …, C. A. Ahern. 2015. Incorporation of non-canonical amino acids. *In* Novel Chemical Tools to Study Ion Channel Biology. C. Ahern and S. Pless, eds. Springer, pp. 119–151.

47. Kratochvil, H. T., M. Maj, …, M. T. Zanni. 2017. Probing the effects of gating on the ion occupancy of the K^+ channel selectivity filter using two-dimensional infrared spectroscopy. *J. Am. Chem. Soc.* 139:8837–8845.

48. Shrivastava, I. H., and M. S. Sansom. 2000. Simulations of ion permeation through a potassium channel: molecular dynamics of KcsA in a phospholipid bilayer. *Biophys. J.* 78:557–570.

49. Paul, F., H. Wu, …, F. Noé. 2019. Identification of kinetic order parameters for non-equilibrium dynamics. *J. Chem. Phys.* 150:164120.

50. Lopes, P. E. M., O. Guvench, and A. D. MacKerell. 2015. Current status of protein force fields for molecular dynamics simulations. *In* Molecular Modeling of Proteins: Methods in Molecular Biology. A. Kukol, ed. Springer, pp. 47–71.

51. Jansen, T. L. C. 2015. NISE3. https://github.com/GHlacour/NISE_2015.

52. Jansen, T. L. C., and J. Knoester. 2006. Nonadiabatic effects in the two-dimensional infrared spectra of peptides: application to alanine dipeptide. *J. Phys. Chem. B.* 110:22910–22916.

53. Jansen, T. L. C., and J. Knoester. 2009. Waiting time dynamics in two-dimensional infrared spectroscopy. *Acc. Chem. Res.* 42:1405–1411.

54. Jansen, T. L. C., B. M. Auer, …, J. L. Skinner. 2010. Two-dimensional infrared spectroscopy and ultrafast anisotropy decay of water. *J. Chem. Phys.* 132:224503.

55. Liang, C., and T. L. C. Jansen. 2012. An efficient N(3)-scaling propagation scheme for simulating two-dimensional infrared and visible spectra. *J. Chem. Theory Comput.* 8:1706–1713.

56. Schmidt, J. R., S. A. Corcelli, and J. L. Skinner. 2004. Ultrafast vibrational spectroscopy of water and aqueous N-methylacetamide: comparison of different electronic structure/molecular dynamics approaches. *J. Chem. Phys.* 121:8887–8896.

57. Jansen, T. L. C., A. G. Dijkstra, …, J. Knoester. 2006. Modeling the amide I bands of small peptides. *J. Chem. Phys.* 125:44312.

58. Kraszewski, S., C. Boiteux, …, C. Girardet. 2009. Determination of the charge profile in the KcsA selectivity filter using *ab initio* calculations and molecular dynamics simulations. *Phys. Chem. Chem. Phys.* 11:8606–8613.

59. Kwac, K., and M. Cho. 2003. Molecular dynamics simulation study of N-methylacetamide in water. I. Amide I mode frequency fluctuation. *J. Chem. Phys.* 119:2247–2255.

60. Ham, S., J.-H. Kim, …, M. Cho. 2003. Correlation between electronic and molecular structure distortions and vibrational properties. II. Amide I modes of NMA–nD_2O complexes. *J. Chem. Phys.* 118:3491–3498.

61. Choi, J.-H., S. Ham, and M. Cho. 2003. Local amide I mode frequencies and coupling constants in polypeptides. *J. Phys. Chem. B.* 107:9132–9138.

62. Bouř, P., and T. A. Keiderling. 2003. Empirical modeling of the peptide amide I band IR intensity in water solution. *J. Chem. Phys.* 119:11253–11262.

63. Carr, J. K., A. V. Zabuga, …, J. L. Skinner. 2014. Assessment of amide I spectroscopic maps for a gas-phase peptide using IR-UV double-resonance spectroscopy and density functional theory calculations. *J. Chem. Phys.* 140:224111.

64. Petti, M. K., J. P. Lomont, …, M. T. Zanni. 2018. Two-dimensional spectroscopy is being used to address core scientific questions in biology and materials science. *J. Phys. Chem. B.* 122:1771–1780.

65. Hamm, P., and M. Zanni. 2011. Concepts and Methods of 2D Infrared Spectroscopy. Cambridge University Press, Cambridge, UK.

66. Bernèche, S., and B. Roux. 2005. A gate in the selectivity filter of potassium channels. *Structure.* 13:591–600.

67. Chakrabarti, N., C. Ing, …, R. Pomès. 2013. Catalysis of Na^+ permeation in the bacterial sodium channel Na(V)Ab. *Proc. Natl. Acad. Sci. USA.* 110:11331–11336.

68. Ke, S., E. N. Timin, and A. Stary-Weinzinger. 2014. Different inward and outward conduction mechanisms in NaVMs suggested by molecular dynamics simulations. *PLoS Comput. Biol.* 10:e1003746.

69. Domene, C., P. Barbini, and S. Furini. 2015. Bias-exchange metadynamics simulations: an efficient strategy for the analysis of conduction and selectivity in ion channels. *J. Chem. Theory Comput.* 11:1896–1906.

70. Callahan, K. M., and B. Roux. 2018. Molecular dynamics of ion conduction through the selectivity filter of the Na_VAb sodium channel. *J. Phys. Chem. B.* 122:10126–10142.

71. Jekhmane, S., J. Medeiros-Silva, …, M. Weingarth. 2019. Shifts in the selectivity filter dynamics cause modal gating in K^+ channels. *Nat. Commun.* 10:123.

72. Langan, P. S., V. G. Vandavasi, …, L. Coates. 2018. Anomalous X-ray diffraction studies of ion transport in K^+ channels. *Nat. Commun.* 9:4540.